Helsinki Conference Proceedings 2019, R. Holmberg et al

SPH modelling of rock blasting: calibration from bench face movement data

M. Bermejo, J. Navarro, J.A. Sanchidrián, P. Segarra & R. Castedo
Universidad Politécnica de Madrid, Madrid, Spain

ABSTRACT: A smoothed particle hydrodynamics (SPH) model has been developed in LS-DYNA for the simulation of the movement of the rock burden. The model is validated with experimental full-scale quarry tests performed within the EU project SLIM. The explosive employed in the tests, an emulsion, has been modelled with the JWL equation of state. The rock was modelled with the RHT constitutive material model. The interaction between explosive and rock is modelled with a node-to-node penalty-based contact. The fracture in the burden and the movement of the rock were monitored by high-speed video recording, with which the initial velocity of the rock face, and the time from the detonation to the onset of the face movement were obtained. These data have been used to calibrate the SPH model. A thorough comparison of the results of tests and simulation are shown.

1 INTRODUCTION

The analysis of the rock movement with video recording is a useful tool in blast design. It can be used as a check of the explosive effect on the rock; inefficiencies in loading, stemming, geometry, timing, etc. are made apparent from the inspection of the recorded images (Chiappetta & Mammele 1987, Pérreault & Morin 2000). The videos provide the necessary data to estimate the trajectory, size and velocity of fragments framed within a specific plane with known coordinates during the movement of the blasted rock (Chiappetta *et al.* 1983). High-speed video recording has been used in this work to record the rock movement, tracking the motion of fragments coming from different height levels on the highwall. From this, the initial velocity of the fragments and the response time, i.e. time between the detonation and the first instance of movement of the bench face, are determined.

Field measurements have been compared with the results of a 2D smoothed particle hydrodynamics model of the rock bench and a blasthole. The model is able to simulate the crack propagation from a blasthole, not easy to achieve with the classical explicit finite element method. This particle method can also simulate with accuracy the detonation in the explosive, and the pressure wave transmitted to the rock.

2 HIGH SPEED VIDEO RECORDING AND DATA ANALYSIS

2.1 Field measurements

The rock movement has been analysed

through high speed video recording during the full-scale test blasts campaign in El Aljibe quarry for the EU project SLIM (Sanchidrián 2018). Blasts were recorded with a high-speed camera (HSC) 'FastCam Sa 3', model 120k C2, manufactured by Photron. It records images at a pre-set frame rate (frames per second, fps), which are saved in an internal memory. Frame rates range from 50 fps to 120,000 fps. Other setups to be considered are related with resolution of the images, shutter, shadows calibration, and type of trigger among others. Due to the limited internal memory (4Gb), it is necessary to keep a balance between the frame rate, the resolution of the images and the total recording time, which must be long enough to record the whole rock movement. In the footage used in this work, the frame rate was 2400 fps, the resolution was 768 × 448 pixels and the recording time was 3.46 s.

2.2 Definition of the reference plane

In order to transform the coordinates in the video images to actual coordinates, a plane is defined in front of the blasthole which burden will be tracked, perpendicular to the free face; for that, surveyed reference points are marked on the crest and on the bench floor, see Figure 1. Rock motion is assumed to take place in that plane.

Surveying was made with a Quarryman ALS Laser system (QLS). To define the perpendicular plane, the QLS is located over the selected blasthole and the direction of the two adjacent blastholes on each side is measured. The perpendicular orientation is obtained by pointing the QLS 90° from the mean azimuth of the previous measurements towards the grade level.

Ideally the camera should be placed so that the line of sight is parallel to the free face. However, this was difficult to achieve in practice, as can be seen in Figure 1, due to the poor visibility of the first part of the blast in the available area to locate the camera. However, using the reference points known coordinates, a transformation system can be calculated to transform coordinates from the video to the reality. Considering that U_C and U_R are local coordinates in the video and in the reality, respectively, within the reference plane defined by targets in the crest and bottom floor of the bench, the transformation is:

$$U_C = A + B \cdot U_R \quad (1)$$

where A is the translation of the reference axes and B is a transformation matrix defined as the product of three matrixes: a rotation matrix of the vertical axis, a scaling factor matrix of the image, i.e. the scaling factor between the distances in the reference plane in the screen and reality, and a skewing matrix over the vertical axis. Solving Equation 1 for U_R:

$$U_R = B^{-1} \cdot (U_C - A) \quad (2)$$

where B^{-1} is the inverse of B.

2.3 Analysis of fragment paths

The trajectory of fragments at different height of the bench and within the defined reference plane are measured at equal time intervals, until they hit the ground, or disappear within the cloud of broken rock and dust. Each fragment position tracked is associated to a time from the video images.

An approximate sample interval considered is around 0.05 s, obtaining between 10 and 30 measurements per rock, i.e., the trajectory of the rock is followed for about 0.5 to 1.5 seconds from the blasthole initiation. Figure 2 shows, as an example, the trajectory followed by a fragment. The grey cross-hairs represent the starting position of the rock, and the white cross-hairs in Figures 2

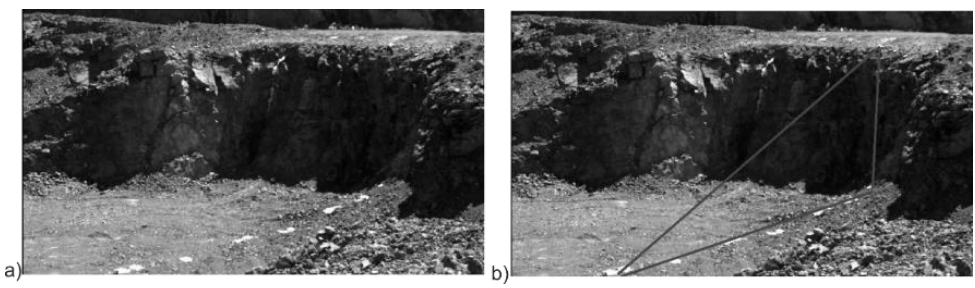

Figure 1. Reference targets.

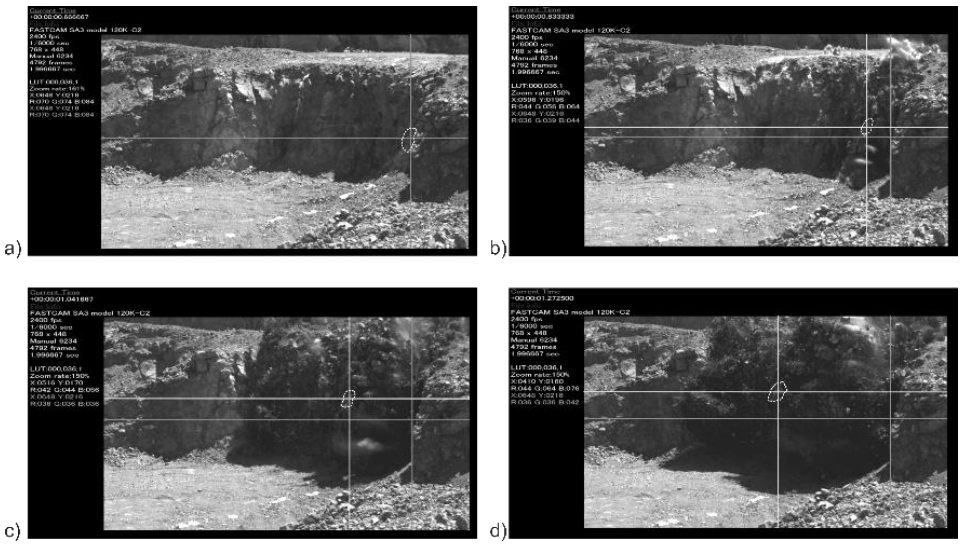

Figure 2. Analysis of the rock trajectory.

b, c and d, the position of the rock at different sample times. Coordinates of the cross position are shown in their respective shade on the left side of the screen. Using Equation 2, real coordinates are calculated.

2.4 Trajectory fitting

The trajectory of each fragment tracked is fit by point trajectory model (Segarra 2004). Figure 3 shows the forces acting on the gravity centre of the fragment; V is the velocity of the target at time t, $\dot{z}$ and $\dot{y}$ are the components of V in the Z (horizontal) and Y (vertical) axis, respectively, θ is the pitch angle, F_D is the aerodynamic drag force, m is the mass of the fragment and g is the acceleration of gravity.

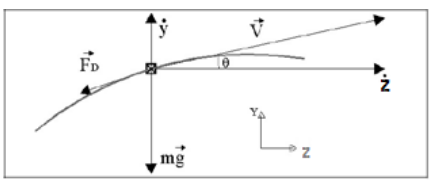

Figure 3. Forces acting on the gravity centre of the rock.

From Figure 3, the following geometrical relations apply:

$$cos\theta = \frac{\dot{z}}{V} = \frac{\dot{z}}{\sqrt{\dot{z}^2+\dot{y}^2}} \quad (3)$$

$$sin\theta = \frac{\dot{y}}{V} = \frac{\dot{y}}{\sqrt{\dot{z}^2+\dot{y}^2}} \quad (4)$$

Applying Newton's second law to the system in Figure 3, and writing the drag force as function of a drag coefficient C_D and fragment cross section S:

$$m\ddot{z} = \frac{-1}{2}\rho V^2 C_D S cos\theta \quad (5)$$

$$m\ddot{y} = -mg - \frac{1}{2}\rho V^2 C_D S sin\theta \quad (6)$$

Replacing Equations 3 and 4 in 5 and 6, respectively:

$$\ddot{z} = \frac{-1}{2}\frac{\rho C_D S}{m}\dot{z}\sqrt{\dot{z}^2+\dot{y}^2} \quad (7)$$

$$\ddot{y} = -g - \frac{1}{2}\frac{\rho C_D S}{m}\dot{y}\sqrt{\dot{z}^2+\dot{y}^2} \quad (8)$$

Equations 7 and 8 form a second order ordinary differential equation system, that can be readily solved for $z(t)$ and $y(t)$. The trajectory obtained is adjusted to the measured one by means of an iterative process in which the two components of the initial velocity are changed until the best fit is obtained. The whole trajectory tracked is used.

The paths measured (already transformed into actual coordinates) and the trajectories calculated are represented in Figure 4a. Figure 4b represents

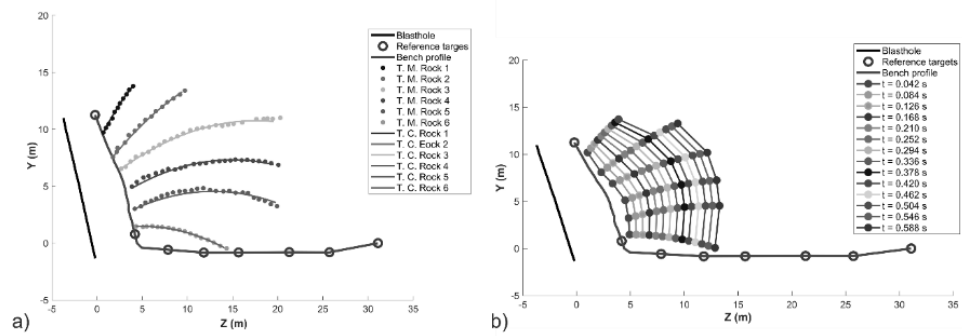

Figure 4. a) Trajectories adjustment; b) Face profiles.

the free face profiles at several times. These profiles are formed by connecting the rock trajectory points (circles) measured at the same time.

Table 1. Height and burden of fragments tracked, velocity and response time.

Fragment	Height rock m	Burden m	Initial velocity m/s	Response time ms
1	9.72	2.47	14.03	23.10
2	7.56	3.30	18.24	23.60
3	6.52	3.40	18.61	23.80
4	4.97	3.83	17.14	24.10
5	3.02	4.10	16.51	24.50

2.5 Determination of the response time

Downhole initiation with electronic detonators was employed. To measure the response time of the rock, i.e. time between the detonator firing to the first movement of the rock, it is necessary to record with the camera the precise moment at which the explosive is detonated. For that, a detonator was located outside the blasthole with the same time that the initiator, so that the initiation time was recorded by the HSC. Since the scatter of this type of detonators is minimal (around 0.1 ms as measured in the tests), both the initiator and the external detonators fire, for all purposes, at the same time.

The initiation of the detonator outside the blasthole generates a flash. Rock trajectories in Figure 4 are measured from the time of this flash or initiation of the explosive. Between the blasthole initiation flash time to the onset of movement of a given spot on the face, there is a short time interval where the rock remains still. The time at which there is a first evidence of movement is visually observed in the video recording, and the time read.

2.6. Results

The height, actual burden from the blasthole at that height, and the initial velocity and response times for five fragments are listed in Table 1.

3 NUMERICAL MODELLING WITH SMOOTHED PARTICLE HYDRODYNAMICS (SPH)

A 2D model with SPH formulation and plane-strain conditions has been used. All SPH particles have approximately equal inter-particle distance of 15 mm in both directions. In the SPH model, the repulsive contact force acting on each particle depends on the linear-spring constant or stiffness. All the SPH interpolations (density, stresses) are carried out inside the local domains of each SPH part. For the interactions between explosive and rock, a node-to-node penalty-based contact is used; this is needed especially when the materials have significantly different densities such as the detonation products and the rock. A "*DEFINE_SPH_TO_SPH_COUPLING" LS-DYNA keyword (Hallquist 2006) is used for the explosive to rock contact.

Tensile (Ganzenmüller *et al.* 2016) and rank-deficient (Dyka *et al.* 1997) instabilities, two problems related to SPH method, are solved through the hourglass control schemes. The tensile instability appears by nonphysical clumping of

particles under conditions of tensile stress. The rank-deficiency problem arises in the nodal integration when the number of integration points is too small such that the solution to the equilibrium equations becomes non-unique due to rank deficiency. Hourglass control locally linearises the deformation field to obtain stable and accurate solutions, without the need to resort to stabilisation via excessive artificial viscosity. The hourglass used within the simulation is the standard LS-DYNA viscous form with the quadratic bulk viscosity coefficient (Q_1) equal to 0.5 and the linear one (Q_2) equal to 1.5.

The model represents a borehole in the bench (Figure 5), loaded with explosive, and the upper part filled with the stemming (in the lighter shade); the rock mass is the dark grey shade. The borehole has and inclination of 11.5º, a length of 12.9 meters and a diameter of 89 mm. The bench has a height of 11.6 meters and an inclination of 32.5º. Even if there are local variations of burden due to the non-planarity of the bench face, the burden increases approximately linearly with depth (see Table 1) and its variability with respect to a theoretical plane is relatively small, so it can be represented fairly accurately with an inclined line for simulation purposes.

A 3.2 metre floor space is modelled, with 11 metres of rock downwards and 23 metres from the crest of the bench backwards. These large dimensions ensure that there are no interferences of numerical, parasitic reflected waves in the domain of interest (although a non-reflecting boundary has been used in the back and in the bottom of the model).

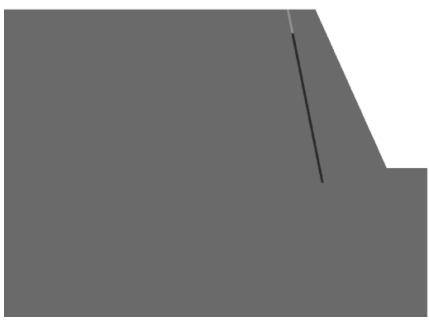

Figure 5. Particle model. Rock in green, explosive in red and stemming in blue.

The rock is described by the RHT model (Borrvall & Riedel 2011). RHT is a macro-scale material model that incorporates features required for a correct dynamic strength description of problems with high strain rates and pressures. The shear strength of the model is described by means of three limit surfaces; the inelastic yield surface, the failure surface and the residual surface, all dependent on the pressure. The post-yield and post-failure behaviours are characterised by strain hardening and damage, respectively, and strain rate effects is an important ingredient in this context. Furthermore, the pressure is governed by the Mie-Grüneisen equation of state together with a porosity-dependent pressure model to describe the pore compaction hardening effects. In our case, where the rock has a very low porosity (water absorption coefficient 0.1 % and very high P-wave velocity, 5800 m/s in lab samples and 5250 m/s in the field), the porosity is negligible and the porosity parameter (the fraction between the density of the matrix material and the rock) is taken as 1 in the initial state (i.e. fully compacted material) and the material behaviour is governed by a conventional equation of state model. The RHT strength model is expressed in terms of the three stress limit surfaces mentioned above. The model is elastic until the stress reaches the initial yield surface, beyond which plastic strains evolve. The plastic strains together with the hardening properties are used to form an effective yield surface by interpolating between the initial yield surface and the failure surface. Similarly, when the stress reaches the failure surface, a parametrised damage model applies, driven by plastic strain, which in turn represents the post-failure stress limit surface by interpolating between the failure surface and the residual friction surface. The relevant parameters of the damage model that require tailoring are D_1, D_2 and ε_p^m (Tu *el al.* 2009), see Table 2. The Hugoniot polynomial coefficients A_1, A_2, A_3 are obtained from the formulation by Xie *et al.* (2017):

$$\begin{aligned} A_1 &= \alpha\rho c^2 \\ A_2 &= \alpha\rho c^2(2s-1) \\ A_3 &= \alpha\rho c^2[(3s-1)(s-1)] \end{aligned} \quad (9)$$

where $\rho = 2714\,kg/m^3$ is the initial density of rock, and c and s are the shock Hugoniot linear expression constants:

$$U_s = c + s \cdot U_p \quad (10)$$

where c=5250 m/s has been chosen equal to the sound speed (assuming that Equation 10 holds at

Table 2. Parameters for the RHT material model.

Parameter	Value	Remarks
Density	2714 kg/m^3	Lab measured
Shear Modulus	41.6 GPa	Lab and field data; elastic relations
Pore crush (B0)	1.2	Equal to the Grüneisen coefficient(1)
Pore crush (B1)	1.2	Equal to the Grüneisen coefficient(1)
Bulk Modulus (T1)	75 GPa	Lab and field data; elastic relations
Bulk Modulus (T2)	0.0 GPa	Ding *et al.* (2013)
Hugoniot parameter (A1)	75 GPa	Eqs. 1
Hugoniot parameter (A2)	90 GPa	Eqs. 1
Hugoniot parameter (A2)	15.5 GPa	Eqs. 1
Failure surface parameter (Af)	1.6	Tu & Lu 2009
Failure surface exponent (nf)	0.61	Tu & Lu 2009
Compressive strength (fc)	182 MPa	Lab tests
Relative shear strength (fs*)	0.18 MPa	Lab(2)
Relative tensile strength (ft*)	0.1 MPa	Lab(2)
Lode Angle (Q0)	0.68	Tu & Lu 2009(3)
Lode Angle (B)	0.0105	Tu & Lu 2009(3)
Compressive reference strain rate	3×10-5 s-1	Ding *et al.* 2013
Compressive break strain rate	3×1025 s-1	Borrvall & Riedel 2011
Tensile reference strain rate	3×10-6 s-1	Ding *et al.* 2013
Yield surface parameter (gc*)	0.53	Borrvall & Riedel 2011
Yield surface parameter (gt*)	0.7	Borrvall & Riedel 2011
Damage parameter (D1)	0.015	Tu & Lu 2009
Damage parameter (D2)	1.0	Tu & Lu 2009
Residual damaged strain (ε_p^m)	8.0×10-4	Tu & Lu 2009
Crush Pressure	182 MPa	(4)
Initial porosity parameter	1.0	Non-porous material

1 The Grüneisen coefficient is approximated as $\gamma = 2s - 1$ (Ding et al. 2013).
2 Shear and tensile strengths normalised with compressive strength; the von Mises criterion for shear strength is used.
3 Strength-reduction parameters.
4 Equal to the compressive strength (fc) since the initial porosity parameter is 1.

low particle velocities). The slope *s* varies for strong rocks (e.g. granite) from about 0.6 to 1.5 depending on the shock range (Sekine *et al*. 1995); we as been chosen *s*=1.1.

Table 2 summarises the parameters used for the RHT model. The basic elastic parameters used are field-measured P-wave velocity and dynamic Poisson ratio, the latter obtained from laboratory values of P- and S-wave velocities (no S- wave velocity is available from the field tests). Other parameters such as shear modulus or bulk modulus are derived from them. Compressive and tensile strength are obtained from laboratory tests.

The stemming was modelled with material '*Mat_Soil_And_Foam'. The density, shear modulus and bulk modulus used are 1650 kg/m^3, 10 MPa and 13.6 GPa respectively.

The explosive is an emulsion with density 1177.5 kg/m^3, velocity of detonation 5448 m/s and detonation pressure calculated at 7.94 GPa. The material "*Mat_High_Explosive_Burn" is used. This material model must be used in combination

Table 3. Parameters for the JWL equation of state.

A (GPa)	B (GPa)	C (GPa)	R1	R2	ω	E0 (GPa)
35.243	4.163	0.406	5.612	1.185	0.37	2.757

with an equation of state to define the detonation products pressure-volume-energy relation. The equation of state used is the Jones-Wilkins-Lee (JWL):

$$P = A\left(1 - \frac{\omega}{R_1 V}\right)e^{-R_1 V} + B\left(1 - \frac{\omega}{R_2 V}\right)e^{-R_2 V} + \frac{\omega E}{V} \quad (11)$$

where A, B, R_1, R_2 and ω are parameters for a given explosive in a given detonation condition (e.g. density, diameter, etc.), P is pressure, E is internal energy per unit initial volume and V is relative volume. The constants have been determined from cylinder test data (Sanchidrián *et al.* 2015, López *et al.* 2018, Castedo *et al.* 2018) where explosive density and velocity of detonation were measured at the values given above. The JWL parameters are reported in Table 3. E_0 is the initial energy available. A single ignition point at the bottom of the blasthole has been used.

4 RESULTS AND DISCUSSION

Figure 6 shows the initial state of the model, together with the map of velocity 30 ms from the initiation of the detonation. No reflected waves from the back or the bottom boundaries are formed, which confirms that the dimensions of the model are sufficient. The free face reflected wave is simulated correctly. A positive velocity gradient from the blasthole to the free face is obtained, whereas velocity decreases steadily backwards and downwards.

The velocity and response time of five fragments formed in the bench face at the same height levels in Table 1 have been calculated from the model results. Clusters of particles moving together have been selected as 'fragments'. These are shown in black with its respective number in Figure 7. The histories of velocity of the particles in each cluster are obtained from the model and the average computed. Figure 8 shows an example of velocity history of a particle and the average velocity of the cluster. There is an initial phase with zero velocity until the P-wave reaches the cluster position, then the velocity ramps up until a steady value is attained; the initial velocity refers to this value. Calculated and test-measured values are given in Table 4. The agreement is quite acceptable and validates the SPH model developed.

In figure 9, the initial velocity of the target fragments is plotted against the ratio of the target height to the bench height, both measured and calculated. Lines are quadratic fits, similar to those shown by Sanchidrián *et al.* (2005).

The response time is taken as the time at which 99 % of the steady velocity (see Figure 8) of the cluster mean velocity is attained. Table 5 shows the comparison between test and model. The model results fall slightly below the measured, though no attempt has been done to tailor the model parameters to match the test data more

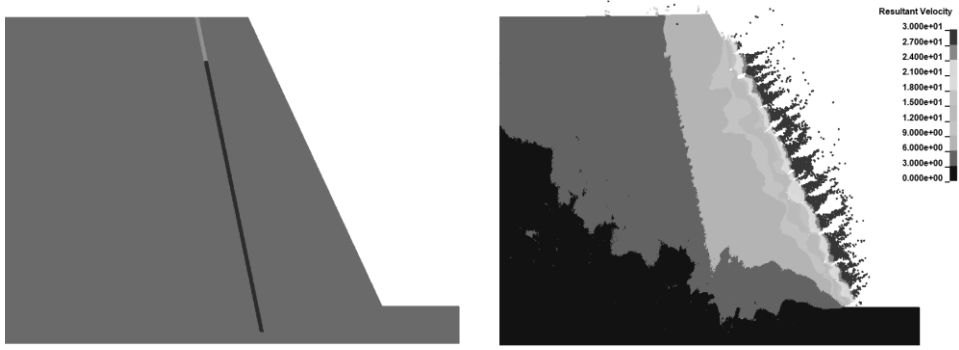

Figure 6. Initial state of the model and map of velocity at 30 ms from initiation.

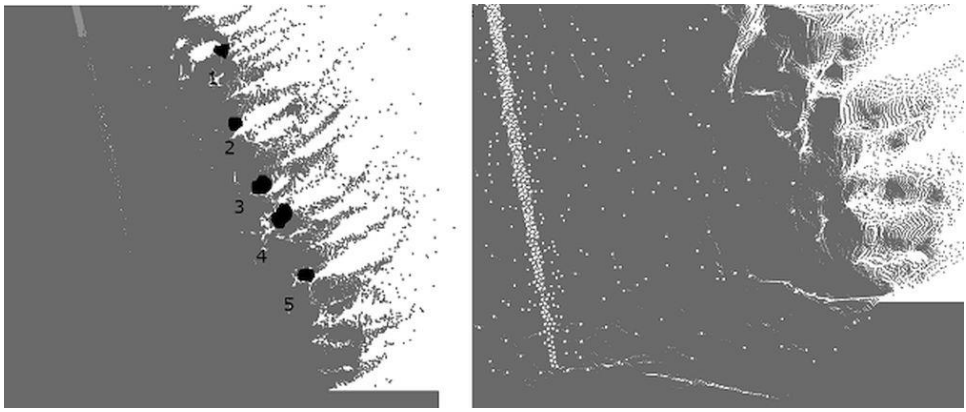

Figure 7. The model 60 ms from initiation. Left: the five fragments selected, Right: detail of the bottom of the borehole; particles ejected and patterns of fractures.

Table 4. Initial velocity. - measured and calculated values.

Fragment	Height of fragment (m)	Burden (m)	Initial velocity, test (m/s)	Initial velocity, model (m/s)	Difference between model and test (%)
1	9.72	2.47	14.03	17.50	24.7
2	7.56	3.30	18.24	18.22	0.11
3	6.52	3.40	18.61	22.00	18.2
4	4.97	3.83	17.14	17.90	4.4
5	3.02	4.10	16.51	17.23	4.3

Table 5. Response time - measured and calculated values.

Fragment	Height of fragment (m)	Burden (m)	Response time, test (ms)	Response time, model (ms)	Error between model and test (%)
1	9.72	2.47	23.1	20.7	-10.5%
2	7.56	3.30	23.6	20.9	-11.4%
3	6.52	3.40	23.8	23.1	-2.9%
4	4.97	3.83	24.1	23.1	-4.1%
5	3.02	4.10	24.5	21.3	-12.9%

accurately. The response time shows a slight direct relation with burden, see Figure 10.

5 CONCLUSIONS

Numerical results indicate that the explosive-to-rock coupled SPH-SPH model can be applied to predict the rock movement, and to calculate the initial velocity of the rock and the response time. The model is validated with data obtained from a full scale quarry test blast. Conclusions on the modelling are:

– 2D SPH models with plane-strain conditions and node-to-node penalty-based contact are useful to simulate the explosive to rock

interaction and the fragments ejection.
– The equal inter-particle distance of 15 mm is appropriate to obtain valid results.

From the analysis of the results, it follows that:

– The face velocity follows a convex function of the target height, being maximum at about mid-height, decreasing towards the top and the floor of the bench. The initial velocity values measured are in the range 15-20 m/s.
– The face response time measured is 23-25 ms from the hole initiation. The response time seems to have a slight direct dependent with burden.

Wave interactions between holes obviously require a 3D model; the 2D model shown in this work is a preparatory exercise for a full 3D SPH-SPH explosive-to-rock interaction model.

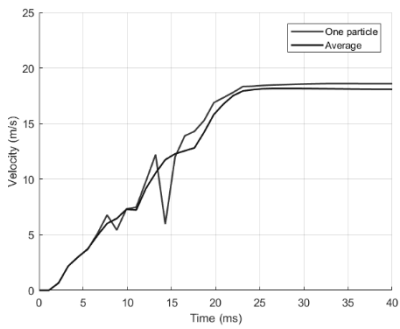

Figure 8. History of velocity, cluster no. 3 in Figure 7. Example of one particle and average of the cluster (smoothed).

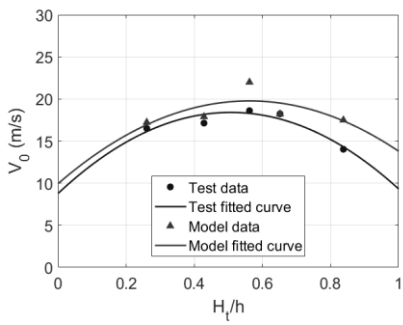

Figure 9. Fragments initial velocity as function of normalised height.

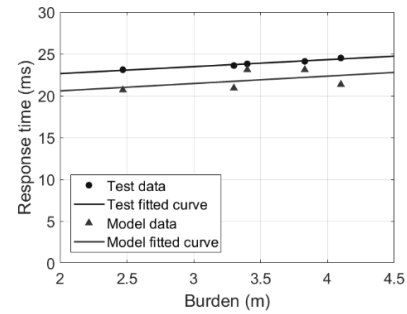

Figure 10. Response time versus burden.

6 ACKNOWLEDGEMENTS

This work is part of the SLIM project, funded by the European Union's Horizon 2020 research and innovation program under Grant agreement no. 730294.

REFERENCES

Borrvall, T. & Riedel, W. 2011. The RHT concrete model in LS-DYNA. In *Proceedings of the 8th European LS-DYNA users conference*, May, Strasbourg - May 2011.

Castedo, R., Natale, M., López, L.M., Sanchidrián, J.A., Santos, A.P., Navarro, J. & Segarra, P. 2018. Estimation of Jones-Wilkins-Lee parameters of emulsion explosives using cylinder tests and their numerical validation. *International Journal of Rock Mechanics and Mining Sciences, 112*: 290-301.

Chiappetta, R.F., Bauer, A., Dailey, P.J. & Burchell, S.L. 1983. The use of high speed motion picture photography in blast evaluation and design. In *Proceedings of the Ninth Conference on explosives and blasting technique*, January 31-February 4, Dallas, Texas. Society of Explosives Engineers.

Chiappetta, R.F. & Mammele, M.E. 1987. Analytical high-speed photography to evaluate air decks, stemming retention and gas confinement in presplitting, reclamation and gross motion applications. In W.L. Fourney & R.D. Dick, *Proc. 2nd Int. Symp. on rock fragmentation by blasting*, Keystone, CO, 23–26 August. Bethel, CT: Society for Experimental Mechanics.

Ding, Y.Q., Tang, W.H., Zhang, R.Q. & Ran, X.W. 2013. Determination and validation of parameters

for Riedel-Hiermaier-Thoma concrete model. *Defence Science Journal* 63(5): 524-530.

Dyka, C.T., Randles, P.W. & Ingel, R.P. 1997. Stress points for tension instability in SPH. *International Journal for Numerical Methods in Engineering* 40(13): 2325-2341.

Ganzenmüller, G.C., Sauer, M., May, M. & Hiermaier, S. 2016. Hourglass control for smooth particle hydrodynamics removes tensile and rank-deficiency instabilities. *The European Physical Journal Special Topics* 225(2): 385-395.

Hallquist, J.O. 2006. *LS-DYNA theory manual*. Livermore Software Technology Corporation, Livermore, CA.

López, L.M., Castedo, R., Sanchidrián, J.A., Natale, M., Santos, A.P., Navarro, J. & Chiquito, M. 2018. Emulsion characterisation with cylinder test and JWL parameters determination. In H. Schunnesson & D. Johansson (eds.) *Proc. 12th Int. Symp. on Rock Fragmentation by Blasting (Fragblast 12)*, 11-13 June, Luleå, Sweden, pp. 431-439.

Pérreault, J.F. & Morin, A. 2000. Optimisation des paramètres de sautage à la Compagnie Minière Québac Cartier. In *23e Session détude sur les techniques de sautage*, Département de mines et métallurgie, 2-3 November 2000, Québec, Canada. Université Laval.

Sanchidrián, J.A. 2018. SLIM: Technology for blasting to improve mining. In H. Schunnesson & D. Johansson (eds.) *Proc. 12th Int. Symp. on Rock Fragmentation by Blasting (Fragblast 12)*, 11-13 June, Luleå, Sweden, pp. 783-793.

Sanchidrián, J.A., Castedo, R., López, L.M., Segarra, P. & Santos, A.P. 2015. Determination of the JWL constants for ANFO and emulsion explosives from cylinder test data. *Central European Journal of Energetic Materials* 12(2): 177-194.

Sanchidrián, J.A., Segarra, P. & López, L.M. 2005. On the relation of rock face response time and initial velocity with blasting parameters. In *Proc. 3rd World Conf. on Explosives and Blasting*, September, Brighton, UK, European Federation of Explosives Engineers, pp. 375-389.

Segarra, P. 2004. Experimental analysis of fragmentation, vibration and rock movement in open pit blasting. *Doctoral Thesis*, Universidad Politécnica de Madrid.

Sekine, T., Duffy, T.S., Rubin, A.M., Anderson, W.W. & Ahrens, T.J. 1995. Shock compression and isentropic release of granite, *Geophys. J. Int.* 120: 247-261.

Tu, Z. & Lu, Y. 2009. Evaluation of typical concrete material models used in hydrocodes for high dynamic response simulations. *International Journal of Impact Engineering* 36(1): 132-146.

Xie, L.X., Lu, W.B., Zhang, Q.B., Jiang, Q.H., Chen, M. & Zhao, J. 2017. Analysis of damage mechanisms and optimisation of cut blasting design under high in-situ stresses. *Tunnelling and Underground Space Technology* 66: 19-33.